FOCUS ISSUE OF SELECTED PAPERS FROM IMLB 2016 WITH INVITED PAPERS CELEBRATING 25 YEARS OF LITHIUM ION BATTERIES

Sodium Alginate: A Water-Processable Binder in High-Voltage Cathode Formulations

Francesca Bigoni, Francesca De Giorgio, Francesca Soavi,* and Catia Arbizzani*,z

Department of Chemistry "Giacomo Ciamician", Alma Mater Studiorum-University of Bologna, 40126 Bologna, Italy

Binders are electrochemically inactive electrode components. However, their chemical and physical nature greatly affects battery performance and plays a key role in electrode integrity and interface reactivity. The binders thus have a strong impact on battery capacity retention and cycle life. Water-processable binders would make the electrode preparation process cheap and environmentally friendly and provide a viable alternative to polyvinylidene difluoride (PVdF). Here we report the use of sodium alginate (SA) as binder for $LiNi_{0.5}Mn_{1.5}O_4$ (LNMO), one of the most promising cathode materials for high-voltage and high-energy LIBs. We demonstrate that electrodes with high mass loading containing SA have excellent specific discharge capacity (120 mAh g^{-1} at C/3 and 100 mAh g^{-1} at 5C) with negligible overpotentials in conventional electrolyte based on ethylene carbonate (EC): dimethyl carbonate (DMC) and 1 M $LiPF_6$, where the reactivity of LNMO is known to negatively affect stability. The electrodes with SA also show a good stability over subsequent cycles of charge and discharge at 1C with capacity retention of 95% and 86% with respect to the initial cycles at the 100th and 200th cycle.

Manuscript submitted September 12, 2016; revised manuscript received October 31, 2016. Published December 5, 2016. This was Paper 924 presented at the Chicago, Illinois, Meeting of the IMLB, June 19–24, 2016. *This paper is part of the Focus Issue of Selected Papers from IMLB 2016 with Invited Papers Celebrating 25 Years of Lithium Ion Batteries.*

Lithium-ion batteries (LIBs) have been on the market for 25 years and recently are being widely used in electric vehicles.[1,2] Research is currently focused on improving the safety and performance of LIBs in terms of gravimetric and volumetric energy and power as well as reducing the costs and toxicity of battery components and of the manufacturing process.[3,4] While the three main active battery components, i.e. anode, cathode and electrolyte, are widely studied, as shown by numerous review papers,[5–8] it is worth noting that such inactive battery components as separators are extremely important in overall operation.[9] The same holds true for the conductive agent (usually carbon black) and the binder that support the electrochemical processes even if present in low weight percentages in electrode composite. The former improves electronic conductivity and, hence, the rate capability of the electrode. The latter acts as glue for active material and the conductive agent and can also improve adhesion with the current collector. Although electrochemically inactive, the chemical and physical nature of polymeric binders can enhance battery performance, control the interface structure of the electrode and has a strong impact on battery capacity retention and cycle life.[10]

The most widely used binder for LIBs is polyvinylidene difluoride (PVdF). While displaying all the desirable binder properties, such as good adhesion strength to the current collector and good electrochemical stability, it can also soak up a large amount of liquid electrolyte, a property that has its pros and cons.[11] A facile penetration of the electrolyte inside the composite electrode results in a high interfacial area of active material in contact with the electrolyte. While this facilitates Li^+ transport, it also promotes unwanted side-reactions. Furthermore, the soaked electrolyte can swell the composite electrode material, resulting in contact loss between particles and in an increase of electrode resistance.[12]

PVdF requires the use of organic solvents like as *N*-methylpyrrolidone (NMP) that are toxic and expensive. Water-processable binders would make the electrode preparation process cheap and environmentally friendly and provide a viable alternative to PVdF. Polyacrylic acid (PAA) is one of the most widely studied water-soluble binders as an alternative to PVdF. This polymer is soluble in both water and in such other organic solvents as ethanol that is more environmentally friendly than NMP. Thanks to the presence of carboxylic acid functional groups, it can form hydrogen bonds with the active material. A derivate of PAA was first studied as a dispersant and a binder for $LiCoO_2$ cathodes in LIBs by Li et al.[13,14] It has subsequently been investigated as a binder for graphite,[15,16] SnCoC[17] and Si[18] anodes and for other cathode materials like $LiMn_2O_4$[19] and $LiFePO_4$.[15,20] Cai et al.[20] reported that $LiFePO_4$ electrodes with PAA binder had greater stability and lower resistance than those with PVdF binder.

Many studies have indicated that water processable cellulose-like materials may be suitable binders for both anode and cathode.[10,19,21,22] The use of carboxymethylcellulose (CMC) as binder for a graphite-based anode material was first described by Lee et al.[23] CMC binder has been proposed also for Si-based electrodes. It can promote the formation of a stable solid electrolyte interface (SEI) layer by acting as a surface modifier and can facilitate networking between the conductive carbon and the Si particles because of its extended structure.[24,25] The presence of carboxylic groups on CMC promotes the formation of hydrogen bonds with hydroxyl groups on Si surfaces, especially at high temperature, which leads to improved stability of the electrode structure.[26]

CMC has also been successfully used in $LiFePO_4$ cathode formulations, with improved capacity retention over cycling.[27] $LiNi_{1/3}Mn_{1/3}Co_{1/3}O_2$ (NMC) cathodes with CMC binder showed improved high rate capability in comparison with electrodes using PVdF.[28,29] High-voltage cathodes based on $LiNi_xMn_{2-x}O_4$ (x = 0.4 and 0.5) and on Li_2MnO_3–$LiMO_2$ displayed improved performance, too.[30,31]

Sodium alginate (SA) is a less widely studied binder. A biopolymer extracted from brown seaweeds, SA contains 1,4-linked β-*D*-mannurate and α-*L*-guluronate which can be arranged to form copolymer or homopolymer dyads. Several combinations are thus possible in nature and depend on the source of the alginate. An important property of this material is that it contains a carboxylic group on each monomeric unit that enables a great number of hydrogen bonds between the binder and the electrode materials. It was first studied as a binder for anodic Si-based materials by Kovalenko et al.[32] Subsequent studies demonstrated its suitability for cathodic materials like $LiNi_{1/3}Mn_{1/3}Co_{1/3}O_2$, $LiMn_2O_4$[29,33,34] and, very recently, for $LiNi_{0.5}Mn_{1.5}O_4$.[35]

One of the crucial challenges in LIB electrode formulation is to identify the best strategy to develop electrodes with high mass loading without penalizing capacity and rate performance which is required for large-size batteries.

*Electrochemical Society Member.
zE-mail: catia.arbizzani@unibo.it

Here we report the use of SA as a binder for $LiNi_{0.5}Mn_{1.5}O_4$ (LNMO) electrodes and focus our work on electrodes with high mass loading. LNMO is one of the most promising cathode materials for LIB use in electric vehicles thanks to its good theoretical capacity (146.7 mAh g^{-1}), high operating voltage (4.7 V vs. Li^+/Li) and good high-rate performance.[36,37] However, its reactivity with conventional electrolytes based on ethylene carbonate (EC): dimethyl carbonate (DMC) and 1 M $LiPF_6$ is well known.[38] We report that the use of SA binder with high LNMO loading enhances the cycling performance of the electrodes with respect to the use of PVdF and offers the advantage of enabling water-process methods for the preparation of high-voltage, high-loading electrodes, a key feature in view of large-size battery production for electric vehicles.

Experimental

Electrode preparation.—The electrodes were prepared by mixing the active material $LiNi_{0.5}Mn_{1.5}O_4$ (LNMO, Nanomyte SP-10, NEI Corporation), the conductive agent C-nergy Super C65 carbon black (C65, Imerys) and the binder sodium alginate (SA, Sigma-Aldrich). Polyvinylidenedifluoride (PVdF, Kynar HSV 900, Arkema) was taken as reference binder.

The composite material (2 g) containing SA was obtained by dissolving the binder in 4 mL of MilliQ water and mixing with a magnetic stir bar for 30 minutes; LNMO was then added and the whole mixed in the planetary mill (PULVERISETTE 6, Fritsch) with tungsten carbide (WC) jar and balls (25 balls, 5 mm diameter) at 250 rpm for 30 minute. Thereafter, C65 was added and 1-hour mixed in the planetary mill. The resulting product was viscous slurry containing 87% LNMO, 10% C65 and 3% SA weight composition. The use of PVdF required a different formulation, and 5% binder content was an optimal value.[39] The composite cathode material containing PVdF with 85% LNMO, 10% C65 and 5% PVdF weight composition was prepared by dry mixing LNMO and C65 with a planetary mill with 25 WC balls in a WC jar at 250 rpm for 1 hour. Subsequently, PVdF powder was added and dry mixed for 1 hour, then 3 mL (for 2 g of composite material) of *N*-methylpyrrolidone (NMP, Sigma-Aldrich, >99%) were added and the whole was mixed for 1 h.

The slurries were deposited on aluminum foil sheets previously etched in KOH 5 wt% for 1 min via mini coater machine (MC 20, Hohsen Corp.) by adjusting the thickness between 6 and 10 mil (150–250 μm). The electrode layers with SA (LNMO_SA) were allowed to dry at room temperature, as a quick drying process would cause the formation of cracks and the loss of adhesion between the composite material and the current collector. Electrodes with PVdF (LNMO_PVdF) were allowed to oven-dry at 60°C overnight. The electrodes LNMO_SA and LNMO_PVdF were obtained by punching the corresponding electrode layers with a 9 mm-diameter puncher. They were pressed at 5 tons for 1 minute with a hydraulic press and dried under dynamic vacuum at 100°C for 16 hours in glass Büchi B-585 oven. The loading of active material per electrode was in the range 6–9 mg cm^{-2}.

Electrochemical tests.—Teflon T-shaped cells (Bola, Bolhender GmbH) were assembled in a dry box (LabMaster SP, MBraun) with argon atmosphere (H_2O < 0.1 ppm, O_2 < 0.1 ppm), with LNMO working electrodes and lithium metal as counter electrode and reference electrode. The electrolyte was 1 M $LiPF_6$ in ethylene carbonate (EC):dimethyl carbonate (DMC) 1:1 (Selectilyte LP30, BASF) and the separator a microfiber glass membrane Whatman GF/D (10 mm diameter). The electrochemical tests were carried out with Perkin-Elmer VMP and Biologic VSP multichannel potentiostat/galvanostats at 30°C. Galvanostatic charge/discharge cycles between 3.5 and 4.8 V vs. Li^+/Li were carried out to evaluate the discharge performance of the cathode materials prepared with the two binders at different current densities and their cycling stability when subjected to repeated charge and discharge cycles. The electrochemical characterization always started with three charge/discharge cycles, with a charge at C/3 constant current (CC), followed by a potentiostatic charge (CV) over 30 minutes or until the attainment of a current corresponding to C/10 and a CC-discharge at C/3. Electrochemical impedance spectroscopy (EIS) measurements on LNMO electrodes in the charged state were also performed in three-electrode mode in the range 100 kHz–100 mHz with a perturbation amplitude of 5 mV, recording 10 points/decade. The electrodes were charged at CC (C/3)-CV at the selected potential vs. Li^+/Li and the spectra taken after at least 1 hour of rest in open circuit for the system to reach equilibrium. EQUIVCRT Boukamp software was used for EIS data fitting.

Physical-chemical characterization.—The morphological and structural properties of SA and PVdF were investigated by scanning electron microscopy (SEM) with a Zeiss EVO 50 microscope equipped with an energy dispersive X-ray analyzer from Oxford INCA Energy 350 system, and by a PANalytical X'Pert PRO powder diffractometer equipped with a X'Celerator detector (CuKa radiation, 40 mA, 40 kV) for X-ray powder diffraction (XRD). SEM and XRD of SA and PVdF films were also recorded after dissolution of the polymers in water and NMP, respectively, i.e. the solvents of electrode slurry formulations.

LNMO_SA and LNMO_PVdF electrodes were also characterized by SEM (surface and cross section) and by porosimetry. The porosimetric analysis was carried out on the composite material detached from the aluminum collector after drying and before pressing the electrode. An ASAP 2020 Micrometrics porosimeter was used and the analyses performed according to BET and DFT methods. The adhesion test (T-peel test) was performed with 4465 of Instron tensiometer on rectangular samples (1 × 2.5 cm) pressed at 10 tons for 2.5 minutes. MagicTM adhesive tape (3M) was applied on the samples and the speed was set at 25 mm min^{-1}. The electrode resistivity was evaluated at room temperature with a four-point probe Jandel multi-height apparatus connected to a Amel 2053 galvanostat/potentiostat and a Hewlett Packard 3478A multimeter on the composite materials deposited on non-conductive substrates (glass or mylar film). Given that the water-based slurry containing SA did not yield homogeneous layers on these support materials, ethylene glycol (Sigma-Aldrich, >99.5%) was used to dissolve the SA binder while maintaining the proportions of the slurry components.

Results and Discussion

Good binding properties of SA were appreciated since electrode preparation. Indeed, LNMO_SA electrodes were easily obtained at low SA content: LNMO_SA electrodes featured a 3% of SA with respect to LNMO_PVdF that contained 5% PVdF.

Figures 1a and 1b show the SEM images of the surface and of the cross-section of pristine LNMO_SA electrode (6–9 mg cm^{-2}). The electrode appears homogeneous, with a good distribution of C65 carbon; the comparison with pristine LNMO_PVdF electrode (Figures 1c and 1d) does not evidence a marked difference in morphology. The BET surface area of both electrode composite materials is ca. 10 m^2 g^{-1} and the DFT analysis shows no difference in their mesoporosity. The different molecular structure and composition of SA and PVdF notably affect the morphology of these powders as shown in Figures 2a and 2b. SA displays particles with irregular shapes and fibrous structure, indicating that it is an amorphous material. On the other hand, PVdF is composed of small, regular spherical particles that testifies to a certain degree of crystallinity, as confirmed by XRD diffractograms in Figure 2c. While SA powder is almost totally amorphous with only traces of short-range order, the diffractogram of PVdF powder shows more defined peaks at 2θ values of 18.2°, 20.0° and 26.6°, typical of the crystalline form II of this polymer.[40] The differences in particle shape and crystallinity do not influence the morphologies of the polymer films resulting from binder dissolution and solvent evaporation. Indeed, the spectra of the dry SA and PVdF films obtained after dispersing the binders in H_2O and NMP, respectively, are almost identical and completely amorphous as shown by the XRD patterns reported in Figure 2c. Electrochemical tests were carried out on the electrodes of the same mass loading with the two different binders. The electrodes

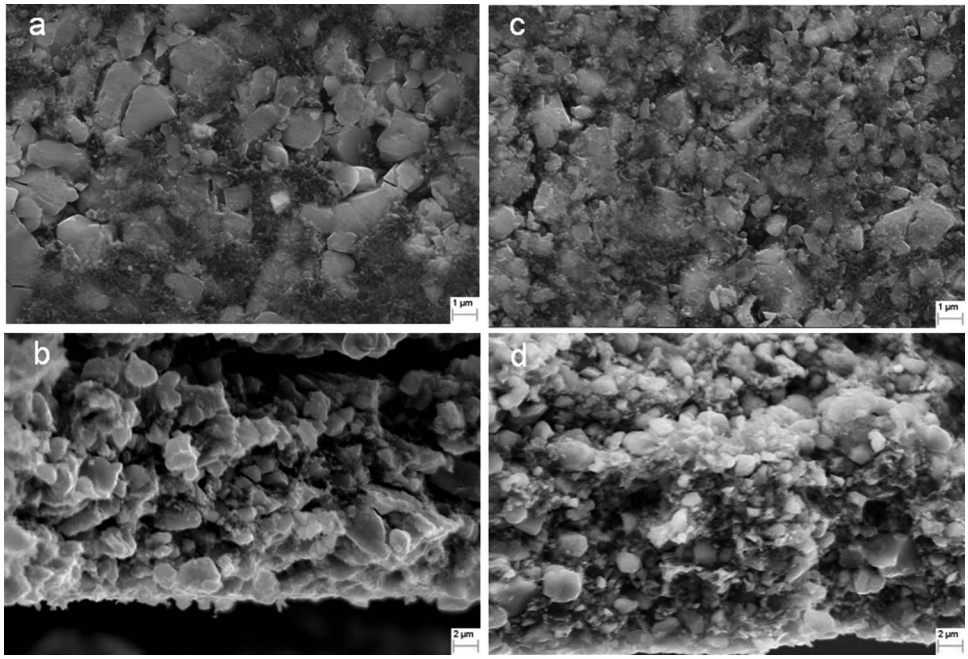

Figure 1. SEM images of pristine electrodes: LNMO_SA (a) surface and (b) cross-section, LNMO_PVdF (c) surface and (d) cross section.

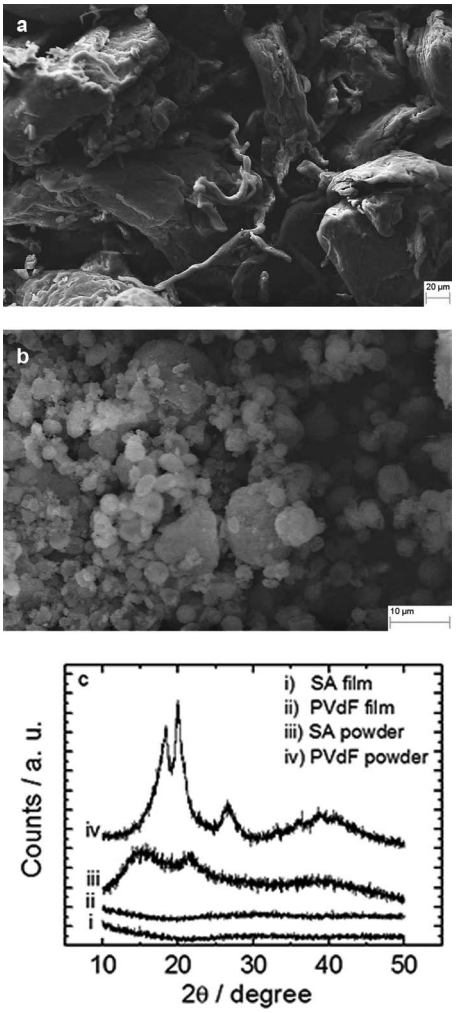

Figure 2. SEM images of (a) SA and (b) PVdF powders and c) XRD diffractogramms of SA (powder and film) and PVdF (powder and film).

underwent charge/discharge cycles in half-cells between 3.5 to 4.8 V vs. Li^+/Li at 30°C. The electrochemical characterization started with three charge/discharge cycles, as indicated in the Experimental part to enable the formation of an effective surface layer that protects LNMO from further reactions with the electrolyte.[38]

The discharge capability of the LNMO_SA electrodes, i.e. their response to progressively increased discharge currents, was evaluated with CC(C/3)-CV charge and CC discharge at increasing C-rate (C/3, C/2, 1C, 2C, 3C, 5C). Three cycles were performed for each C-rate and three additional cycles with CC discharge at C/3 were carried out at the end of the test to assess whether the cell recovered initial conditions. Figure 3 shows the discharge capacity and the percentage of recovered capacity, i.e. the ratio between the discharge capacity and the charge capacity for each cycle of LNMO_SA. The results are compared to those of LNMO_PVdF. The specific capacity of the LNMO_SA and LNMO_PVdF electrodes are quite similar and close to the practical one of LNMO reported in the technical data sheet (130 mAh g^{-1} at C/10). The LNMO_SA and LNMO_PVdF electrodes have similar resistivity, 0.47 ohm cm and 0.76 ohm cm, respectively. The slightly lower resistivity of the former is probably due to the lower amount of binder, i.e. of non-conductive material being the binder-to-carbon black ratio 0.3 for LNMO_SA and 0.5 for LNMO_PVdF.

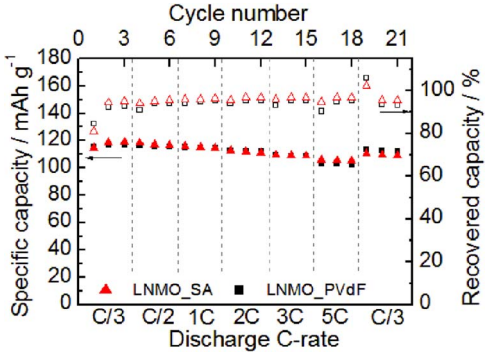

Figure 3. Specific discharge capacity and recovered capacity upon CC(C/3)-CV charge and CC discharge of LNMO_SA (8.1 mg_{LNMO} cm^{-2}) and LNMO_PVdF (8.3 mg_{LNMO} cm^{-2}).

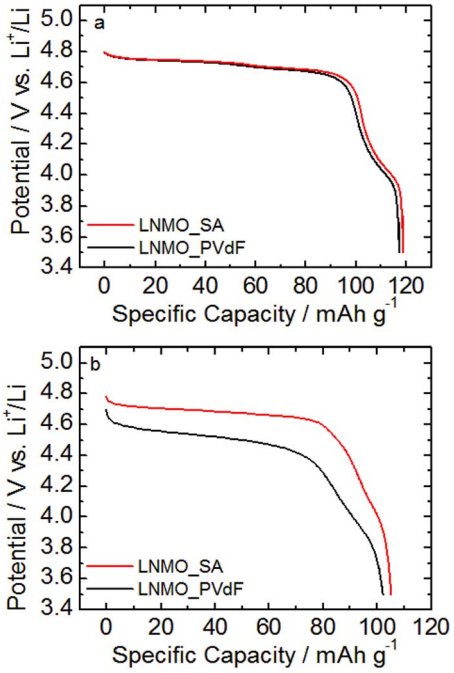

Figure 4. Discharge potential profiles of LNMO_SA (8.1 mg_{LNMO} cm^{-2}) and LNMO_PVdF (8.3 mg_{LNMO} cm^{-2}) electrodes: (a) 3rd discharge at C/3, (b) 3rd discharge at 5C.

A lower binder-to-carbon ratio might favor electric contact between carbon and LNMO. The recovered capacity is good for each material. The first cycle shows a recovered capacity lower than that of the subsequent cycles, with values between 80% and 85%. This is due to the formation of a passivation layer on the surface of the electrodes (both LNMO and Li) caused by the degradation reaction of LP30.[38] By contrast, the first of the last three cycles at C/3 shows a recovered capacity greater than 100%. The reason for this is that the charging processes is not much affected by kinetics when the charging current is maintained at C/3 and the constant current step is followed by the constant potential step. With the increase of the discharge current, a certain amount of charge remains trapped in the electrode, causing the lowering of the discharge capacity. When, at the end of the test, the discharge is carried out at low current, there are fewer kinetic limitations and the trapped charge is delivered.

Despite the similarity in the behavior of electrodes with SA and PVdF during the discharge capability test, differences are evinced in potential profiles. Figure 4 shows the discharge potential profiles of the electrodes at low and high currents (C/3 and 5C). While at C/3 LNMO_SA and LNMO_PVdF have almost superimposed profiles (Fig. 4a), at 5C LNMO_SA displays a lower overvoltage than LNMO_PVdF (Fig. 4b). This is a very important feature for the development of LIBs operating at high C-rates. Indeed, the higher discharge potential profile of LNMO_SA would provide a higher energy of the full cell compared to LNMO_PVdF.

Stability tests were carried out by CC-CV/CC charge/discharge cycles at 1C after five galvanostatic cycles CC-CV/CC at C/3. Figure 5 demonstrates the very high stability of LNMO_SA electrode: it maintained 95% of specific capacity after 100 cycles and 86% after 200 cycles. In the same cycling conditions LNMO_PVdF is less stable displaying a 89% recovered charge after 85 cycles.[41] The Figure also displays the potential profiles of the 1st and the 100th cycle at 1C (i.e. the 5th and 105th total cycles) of LNMO_SA that shows a low increment of the discharge overpotential over cycling. The coulombic efficiency was nearly constant at ca. 98%. However, some scattered values were evident after the 100th. One reason for these scattered values may be the rupture of the SEI passivation layers on LNMO and on Li electrodes over cycling. In this case the

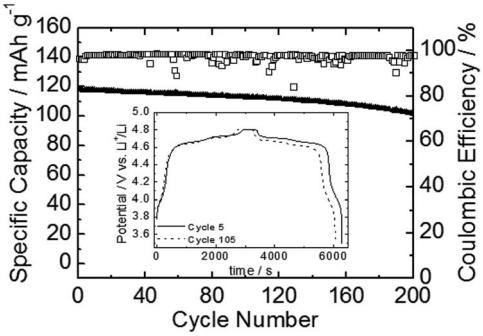

Figure 5. Discharge capacity over repeated CC-CV charge and CC discharge cycles and charge/discharge potential profiles at 1C of LNMO_SA (7.1 mg_{LNMO} cm^{-2}).

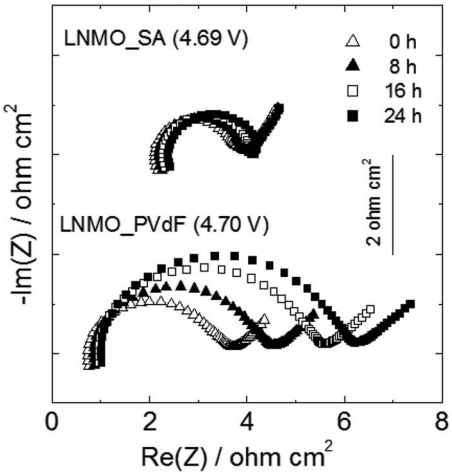

Figure 6. Impedance spectra from 100 kHz to 0.1 Hz of LNMO_SA and LNMO_PVdF recorded in OCV after charge at potential of 4.70 V vs. Li^+/Li at different rest time.

charging process also comprises the charge involved in building new layers so that charge capacity values are much higher than those of discharge capacity. From a chemical point of view, the good stability of LNMO_SA can be attributed to the presence of carboxylic groups in each monomer unit of SA. These groups form ester-like chemical bonds with hydroxyl groups on the surface of the active materials that favor particle cohesion.[19] In addition, the passive layer that usually forms on the electrode surface strictly depends on the nature of the binder.[20,35,42]

To investigate the electrode/electrolyte interface reactivity, electrochemical impedance spectra at different times after charge at 4.70 V vs. Li^+/Li (CC-CV) were taken in OCV and are reported in Figure 6. The Nyquist plots of the charged electrodes feature a high frequency semicircle that represents the solid-electrolyte interface resistance (R_{SEI}). The intercept on the Z real axis at the highest frequency is the uncompensated resistance (R_u). The equivalent circuit that models electrode response is described in Scheme 1 and deeply discussed in the following paragraph. LNMO_SA displays a

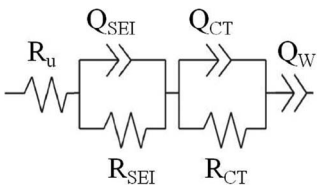

Scheme 1. Equivalent circuit used for the fitting of the EIS data.

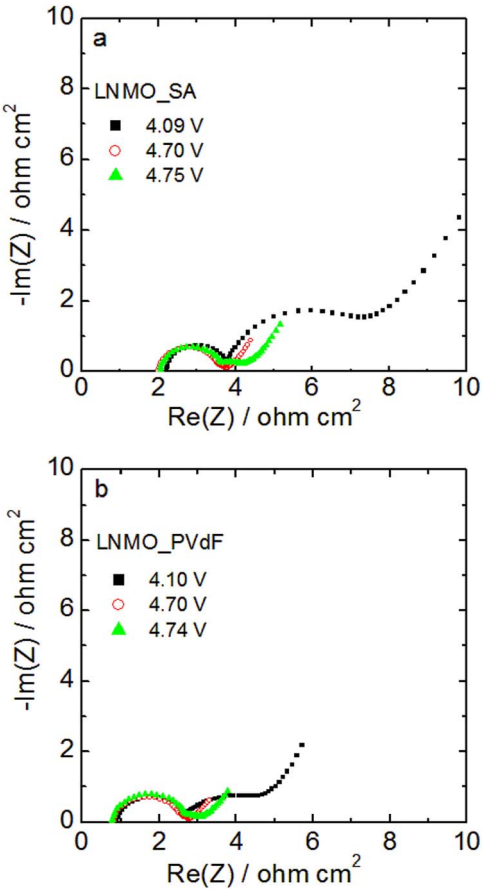

Figure 7. Impedance spectra from 100 kHz to 0.1 Hz of (a) LNMO_SA and (b) LNMO_PVdF recorded after charge (4th cycle) at different potentials vs. Li^+/Li.

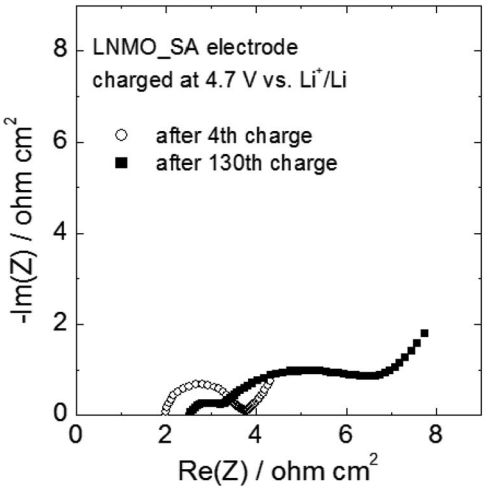

Figure 8. Impedance spectra from 100 kHz to 0.1 Hz of LNMO_SA recorded in OCV at potential of 4.70 V vs. Li^+/Li after the 4th and 130th charge during cycling stability tests.

slight increase of the total resistance over time that is mainly related to the increase in R_u. LNMO_PVdF, by contrast, almost doubles the total resistance in 24 h. Specifically, R_{SEI} increases, thus demonstrating higher interface reactivity of LNMO_PVdF than LNMO_SA. The slightly higher R_u displayed by LNMO_SA electrodes could be ascribed to poorer adhesion of LNMO to Al current collector than that of LNMO_PVdF electrodes. This was confirmed by T-peel test. The adhesive strengths to the aluminum current collectors for the LNMO composite electrodes were 0.14 and 0.38 N cm^{-1} for electrodes with SA and PVdF, respectively. However, this feature does not seem to affect LNMO_SA electrode performance to any great extent, but it is worth improving.

To evince the effect of the SEI formation on the LNMO-based electrodes over cycling, EIS of the LNMO_SA and LNMO_PVdF electrodes was carried out at different potentials after the initial 3 charge/discharge cycles (Figure 7) and at 4.70 V vs. Li^+/Li after 130 cycles (Figure 8). The spectra reported in Figure 7 were collected after having charged the electrodes (4th charge process) at 1C up to 4.10 V and after a rest period of 1 hour in open circuit. The electrodes, which were not discharged at the end of the impedance measurement, were further charged up to 4.70 V and the spectra were collected after the 1h-rest. The electrodes were similarly further charged up to 4.77 V and the impedance measurements performed. The open circuit potentials are reported in Figure 7. The electrodes were then discharged and the stability tests continued. The spectra in Figures 7a (LNMO_SA) and 7b (LNMO_PVdF) display one high frequency semicircle with a diameter (R_{SEI}) that is not affected by the potential value and is ascribed to the solid electrolyte interface. The medium frequency semicircle is related to the charge transfer phenomenon with a diameter that corresponds to the charge transfer resistance (R_{CT}) and increases at low potential. The low frequency line at almost 45° (Q_W) is related to Li^+ diffusion in the solid electrode. Impedance spectra of LNMO_SA were also collected in the charged state after repeated cycles at 1C and shown in Figure 8. The electrodes were charged at 4.70 V vs. Li^+/Li and the spectra taken after 2h-rest in open circuit. The spectra were analyzed with the equivalent circuit $R_U(R_{SEI}Q_{SEI})(R_{CT}Q_{CT})Q_W$ shown in Scheme 1, where R_U is the uncompensated resistance and Q indicates the constant phase element, whose impedance is $Z_{CPE}(\omega) = Q^{-1}(j\omega)^{-a}$, and represents an ideal capacitance if a = 1 and a Warburg element if a = 0.5. The results of the fitting analyses of the spectra are listed in Table I. The data evidence that LNMO_SA impedance increase upon cycling is mainly related to the R_{CT} component. At 130th cycle the R_{SEI} contribution is negligible, thus suggesting the formation of a thin SEI layer and explaining the good cycling performance. For a comparison it has to be mentioned that in the case of LNMO_PVdF both R_{SEI} and R_{CT} significantly increase over cycling. Indeed, we reported that after 27th and 87th cycle R_{SEI} and R_{CT} change, respectively, from 5.4 to 11.7 ohm cm^2 and from 12.0 to 32.0 ohm cm^2.[39]

Passivation layers on LNMO_SA and LNMO_PVdF were investigated by SEM. Specifically, the cells were disassembled after the cycling stability test and the electrodes were analyzed by SEM after being washed with DMC to remove salt traces. The SEM images (surface and cross-section) of these electrodes after cycling are shown

Table I. Fitting parameters of the impedance spectra of Figure 8 of the LNMO_SA electrodes after 4th and 130th charge at 4.7 V vs. Li^+/Li.

Cycle	R_u Ω cm^2	R_{SEI} Ω cm^2	R_{CT} Ω cm^2	Q_{SEI} F $s^{(a-1)}$ cm^{-2}	Q_{CT} F $s^{(a-1)}$ cm^{-2}	Q_W F $s^{(a-1)}$ cm^{-2}
4	1.97 ± 0.04	1.3 ± 0.1	0.5 ± 0.2	$(5.0 \pm 0.7) \cdot 10^{-5}$ a = 0.95 ± 0.02	$(6 \pm 1) \cdot 10^{-2}$ a = 0.46 ± 0.08	1.28 ± 0.02 a = 0.62 ± 0.01
130	2.59 ± 0.07	0.56 ± 0.02	3.53 ± 0.07	$(9 \pm 2) \cdot 10^{-5}$ a = 0.85 ± 0.03	$(1.76 \pm 0.05) \cdot 10^{-2}$ a = 0.60 ± 0.01	0.64 ± 0.02 a = 0.59 ± 0.02

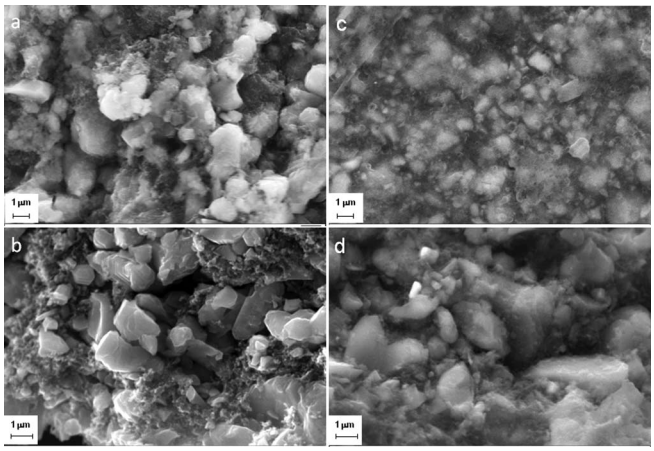

Figure 9. SEM images of electrodes after the cycling stability test: LNMO_SA (a) surface and (b) cross-section, LNMO_PVdF (c) surface and (d) cross section.

in Figure 9. The SEM images show that the LNMO_SA electrode (a, surface and b, cross-section) maintained the same compact structure after cycle life test. The LNMO crystals were well preserved as demonstrated by the hexagonal faces that are evident in several LNMO particles (Figure 9a). SEM images show a slight morphology change in the LNMO_PVdF electrode (c, surface and d, cross-section). In these cycled electrodes the LNMO particle boundaries are smoothed as if covered by a thick SEI layer.

The binder may affect the electrolyte permeation inside the composite material, thereby favoring Li^+ transport but also enhancing the electrolyte reactions on LNMO particles. Therefore, the higher SEI thickness of LNMO_PVdF compared to LNMO_SA can be explained by a higher electrolyte uptake of PVdF than SA. On the other hand, the electrolyte uptake and swelling properties of PVdF, which are due to its flexible linear chains, are well known and exploited for the preparation of solid electrolytes and separators.[11,42] In effect, we found that SA swelling in presence of LP30 electrolyte is not so high and this is due to its more rigid structure. The difference in electrolyte uptake of the two binders is shown in Figure 10. An equal amount of binders (230 mg) was added to the same volume of LP30. The addition of 0.2 mL of electrolyte soaks the SA binder completely but only a small portion of PVdF, which promptly formed a gel. Adding 0.4 mL more (0.6 mL total) of LP30 electrolyte completed gel formation of the entire amount of PVdF but this addition remained as surnatant over SA. While SA is wetted without showing any evident swelling, PVdF is able to soak up a greater volume of electrolyte and readily swells forming a gel. Hence, SA could prevent the massive infiltration of electrolyte into the electrode and this improves the cycling stability of the electrode.

Conclusions

Water-processable SA can be successfully used in high-potential electrode formulations based on LNMO. SA-based electrodes with relatively high mass loadings and high active material percentages were prepared and their performance was compared to that of electrodes containing the conventional PVdF binder. LNMO_SA electrodes showed excellent specific discharge capacity (120 mAh g^{-1} at C/3, close to practical capacity of 130 mAh g^{-1} at C/10) even at very high currents where a specific capacity of about 100–105 mAh g^{-1} was delivered at 5C with negligible overpotentials. By contrast, overpotentials significantly increased at 5C for electrodes with PVdF. The electrodes with SA showed good stability over subsequent cycles of charge and discharge at relatively high current (1C), showing a discharge capacity at the 100th and 200th cycle that was 95% and 86% of the initial one. The poor swelling ability of SA makes LNMO_SA electrodes less susceptible to a massive electrolyte penetration and, hence, to degradation and passivation processes. Therefore, the high-potential LNMO cathodes with high active material mass loading have good electrochemical performance when prepared using SA as binder. Further optimization of binder, conductive material and active material percentages, with particular attention to the slurry formation procedure and physical chemical properties, especially for the scaling up and automation of the coating process, would lead to notable improvements.

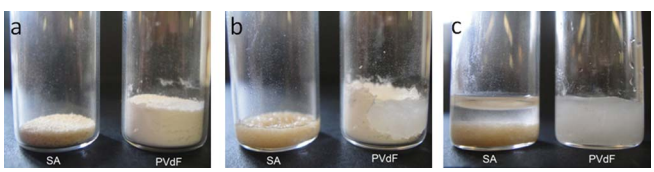

Figure 10. SA and PVdF powders (a) dry and after the addition of (b) 0.2 mL and (c) 0.6 mL of LP30.

Acknowledgments

The authors thank ENEA and Italian Ministry of Economic Development for financial support under the National Program "Electric System Research – Cathode materials for Li-ion high-voltage batteries". The authors are grateful to Prof. M. L. Focarete (University of Bologna) for the adhesion tests and Dr. Fabrizio Tarterini (University of Bologna) for the SEM images and to both for the fruitful discussions.

References

1. C. Pillot, Lithium-Ion Battery Market Expansion Beyond Consumer and Automotive, AABC 2015 January 26–29 Mainz, Germany. http://www.avicenne.com/articles_energy.php (last access 07/07/16).
2. O. Gröger, H. A. Gasteiger, and J.-P. Suchslandc, Review—Electromobility: Batteries or Fuel Cells?, *J. Electrochem. Soc.*, **162**, A2605 (2015).
3. V. Etacheri, R. Marom, R. Elazari, G. Salitra, and D. Aurbach, Challenges in the development of advanced Li-ion batteries: a review, *Energy Environ. Sci.*, **4**, 3243 (2011).
4. A. Manthiram, Materials Challenges and Opportunities of Lithium Ion Batteries. *J. Phys. Chem. Lett.*, **2**, 176 (2011).
5. S. Goriparti, E. Miele, F. De Angelis, E. Di Fabrizio, R. Proietti Zaccaria, and C. Capiglia, Review on recent progress of nanostructured anode materials for Li-ion batteries, *J. Power Sources*, **257**, 421 (2014).
6. P. Rozier and J. M. Tarascon, Review—Li-Rich Layered Oxide Cathodes for Next-Generation Li-Ion Batteries: Chances and Challenges, *J. Electrochem. Soc.*, **162**, A2490 (2015).
7. M. Marcinek, J. Syzdek, M. Marczewski, M. Piszcz, L. Niedzicki, M. Kalita, A. Plewa-Marczewska, A. Bitner, P. Wieczorek, T. Trzeciak, M. Kasprzyk, P. Łężak, Z. Zukowska, A. Zalewska, and W. Wieczorek, Electrolytes for Li-ion transport – Review, *Solid State Ionics*, **276**, 107 (2015).
8. K. Xu, Electrolytes and Interphases in Li-Ion Batteries and Beyond, *Chem. Rev.*, **114**, 11503 (2014).
9. P. Arora and Z. Zhang, Battery Separators, *Chem. Rev.*, **104**, 4419 (2004).
10. S. Chou, Y. Pan, J. Wang, H. Liu, and S. Dou, Small things make a big difference: binder effects on the performance of Li and Na batteries, *Phys. Chem. Chem. Phys.*, **16**, 20347 (2014).
11. J. Saunier, F. Alloin, J. Y. Sanchez, and B. Barriére, Plasticized microporous poly (vinylidene fluoride) separators for lithium-ion batteries. I. Swelling behavior of dense membranes with respect to a liquid electrolyte—Characterization of the swelling equilibrium, *J. Polym. Sci., Part B: Polym. Phys.*, **42**, 2308 (2004).
12. S. Komaba, K. Shimomura, N. Yabuuchi, T. Ozeki, H. Yui, and K. Konno, Study on polymer binders for high-capacity SiO negative electrode of Li-ion batteries, *J. Phys. Chem. C*, **115**, 13487 (2011).
13. C.-C. Li, J.-T. Lee, C.-Y. Lo, and M.-S. Wu, Effects of PAA-NH_4 Addition on the Dispersion Property of aqueous $LiCoO_2$ slurries and the cell performance of as-prepared $LiCoO_2$ cathodes, *Electrochem. Solid-State Lett.*, **8**, A509 (2005).
14. C.-C. Li, J.-T. Lee, and X.-W. Peng, Improvements of dispersion homogeneity and cell performance of aqueous-processed $LiCoO_2$ cathodes by using dispersant of PAA–NH_4, *J. Electrochem. Soc.*, **153**, A809 (2006).
15. J. Chong, S. Xun, H. Zheng, X. Song, G. Liu, P. Ridgwaya, J. Q. Wang, and V. S. Battaglia, A comparative study of polyacrylic acid and poly(vinylidene difluoride) binders for spherical natural graphite/$LiFePO_4$ electrodes and cells, *J. Power Sources*, **196**, 7707 (2011).

16. S. Komaba, K. Okushi, T. Ozeki, H. Yui, Y. Katayama, T. Miura, T. Saito, and H. Groult, Polyacrylate modifier for graphite anode of lithium-ion batteries, *Electrochem. Solid-State Lett.*, **12**, A107 (2009).
17. J. Li, D.-B. Le, P. P. Ferguson, and J. R. Dahn, Lithium polyacrylate as a binder for tin–cobalt–carbon negative electrodes in lithium-ion batteries, *Electrochim. Acta*, **55**, 2991 (2010).
18. A. Magasinski, B. Zdyrko, I. Kovalenko, B. Hertzberg, R. Burtovyy, C. F. Huebner, T. F. Fuller, I. Luzinov, and G. Yushin, Toward efficient binders for Li-ion battery Si-based anodes: polyacrylic acid, *ACS Appl. Mater. Interfaces*, **2**, 3004 (2010).
19. Z. Zhang, T. Zeng, Y. Lai, M. Jia, and J. Li, A comparative study of different binders and their effects on electrochemical properties of $LiMn_2O_4$ cathode in lithium ion batteries, *J. Power Sources*, **247**, 1 (2014).
20. Z. P. Cai, Y. Liang, W. S. Li, L. D. Xing, and Y. H. Liao, Preparation and performances of $LiFePO_4$ cathode in aqueous solvent with polyacrylic acid as a binder, *J. Power Sources*, **189**, 547 (2008).
21. K. A. Seid, J. C. Badot, O. Dubrunfaut, S. Levasseur, D. Guyomard, and B. Lestriez, Influence of the carboxymethyl cellulose binder on the multiscale electronic transport in carbon–$LiFePO_4$ nanocomposites, *J. Mater. Chem.*, **22**, 24057 (2012).
22. G. T. Kim, S. S. Jeong, M. Joost, E. Rocca, M. Winter, S. Passerini, and A. Balducci, Use of natural binders and ionic liquid electrolytes for greener and safer lithium-ion batteries, *J. Power Sources*, **196**, 2187 (2011).
23. J.-H. Lee, U. Paik, V. A. Hackley, and Y.-M. Choi, Effect of carboxymethyl cellulose on aqueous processing of natural graphite negative electrodes and their electrochemical performance for lithium batteries, *J. Electrochem. Soc.*, **152**, A1763 (2005).
24. J. Li, R. B. Lewis, and J. R. Dahn, Sodium carboxymethyl cellulose A potential binder for Si negative electrodes for Li-ion batteries, *Electrochem. Solid State Lett.*, **10**, A17 (2007).
25. B. Lestriez, S. Bahri, I. Sandu, L. Roué, and D. Guyomard, On the binding mechanism of CMC in Si negative electrodes for Li-ion batteries, *Electrochem. Commun.*, **9**, 2801 (2007).
26. F. Luo, B. Liu, J. Zheng, G. Chu, K. Zhong, H. Li, X. Huang, and L. Chen, Review—Nano-silicon/carbon composite anode materials toward practical application for next generation Li-ion batteries, *J. Electrochem. Soc.*, **162**, A2509 (2015).
27. S. F. Lux, F. Schappacher, A. Balducci, S. Passerini, and M. Winter, Low cost, environmentally benign binders for lithium-ion batteries, *J. Electrochem. Soc.*, **157**, A3205 (2010).
28. N. Loeffler, J. von Zamory, N. Laszczynski, I. Doberdo, G.-T. Kim, and S. Passerini, Performance of $LiNi_{1/3}Mn_{1/3}Co_{1/3}O_2$/graphite batteries based on aqueous binder, *J. Power Sources*, **248**, 915 (2014).
29. J. Xu, S. L. Chou, Q. F. Gu, H. K. Liu, and S. X. Dou, The effect of different binders on electrochemical properties of $LiNi_{1/3}Mn_{1/3}Co_{1/3}O_2$ cathode material in lithium ion batteries, *J. Power Sources*, **225**, 172 (2013).
30. Z. L. Wang, N. Dupre, A. C. Gaillot, B. Lestriez, J. F. Martin, L. Daniel, S. Patoux, and D. Guyomard, CMC as a binder in $LiNi_{0.4}Mn_{1.6}O_4$ 5 V cathodes and their electrochemical performance for Li-ion batteries, *Electrochim. Acta*, **62**, 77 (2012).
31. J. Li, R. Klöpsch, S. Nowak, M. Kunze, M. Winter, and S. Passerini, Investigations on cellulose-based high voltage composite cathodes for lithium ion batteries, *J. Power Sources*, **196**, 7687 (2011).
32. I. Kovalenko, B. Zdyrko, A. Magasinski, B. Hertzberg, Z. Milicev, and R. Burtovyy, A major constituent of brown algae for use in high-capacity Li-ion batteries, *Science*, **334**, 75 (2011).
33. M.-H. Ryou, S. Hong, M. Winter, H. Lee, and W. Choi, Improved cycle lives of $LiMn_2O_4$ cathodes in lithium ion batteries by an alginate biopolymer from seaweed, *J. Mater. Chem. A*, **1**, 15224 (2013).
34. J. Li, Y. Zhao, N. Wang, Y. Ding, and L. Guan, Enhanced performance of a MnO_2–graphene sheet cathode for lithium ion batteries using sodium alginate as a binder, *J. Mater. Chem.*, **22**, 13002 (2012).
35. W.-Y. Chou, Y.-C. Jin, J.-G. Duh, C.-Z. Lu, and S.-C. Liao, A facile approach to derive binder protective film on high voltage spinel cathode materials against high temperature degradation, *Appl. Surf. Sci.*, **355**, 1272 (2015).
36. S. Patoux, L. Daniel, C. Bourbon, H. Lignier, C. Pagano, F. Le Cras, S. Jouanneau, and S. Martinet, High voltage spinel oxides for Li-ion batteries: From the material research to the application, *J. Power Sources*, **189**, 344 (2009).
37. J. H. Kim, N. P. Pieczonka, and L. Yang, Challenges and approaches for high-voltage spinel lithium-ion batteries, *ChemPhysChem.*, **15**, 1940 (2014).
38. D. Aurbach, B. Markovsky, Y. Talyossef, G. Salitra, H.-J. Kim, and S. Choi, Studies of cycling behavior, ageing, and interfacial reactions of $LiNi_{0.5}Mn_{1.5}O_4$ and carbon electrodes for lithium-ion 5-V cells, *J. Power Sources*, **162**, 780 (2006).
39. C. Arbizzani, L. Da Col, F. De Giorgio, M. Mastragostino, and F. Soavi, Reduced graphene oxide in cathode formulations based on $LiNi_{0.5}Mn_{1.5}O_4$, *J. Electrochem. Soc.*, **162**, A2174 (2015).
40. M. Tazaki, R. Wada, M. Okabe, and T. Homma, Crystallization and gelation of poly(vinylidene fluoride) in organic solvents, *J. Appl. Polym. Sci.*, **65**, 1517 (1997).
41. F. Bigoni, F. De Giorgio, F. Soavi, and C. Arbizzani, New formulations of high-voltage cathodes for Li-ion batteries with water-processable binders, *ECS Transactions*, **73**, 249 (2016).
42. J. Y. Song, Y. Y. Wang, and C. C. Wan, Conductivity study of porous plasticized polymer electrolytes based on poly(vinylidene fluoride) - A comparison with polypropylene separators, *J. Electrochem. Soc.*, **147**, 3219 (2000).